Solid Earth Discuss., 6, 2759–2778, 2014
www.solid-earth-discuss.net/6/2759/2014/
doi:10.5194/sed-6-2759-2014

Solid Earth
Discussions
Open Access

An improved approach to estimate large-gradient deformation using high resolution TerraSAR-X data

D. Liu[1], R. Chen[2], B. Riedel[1], and W. Niemeier[1]

[1]Institute of Geodesy and Photogrammetry, Braunschweig, Germany
[2]Institute of Electronics, Chinese Academy of Sciences, Beijing, China

Received: 4 August 2014 – Accepted: 21 August 2014 – Published: 17 September 2014

Correspondence to: D. Liu (donglie.liu@tu-bs.de)

Published by Copernicus Publications on behalf of the European Geosciences Union.

Abstract

Interferometric Synthetic Aperture Radar (InSAR) has shown unique capabilities in numerous applications for deformation monitoring. However, InSAR will lose effectiveness with large-gradient deformation due to the limitation of maximum detectable phase gradient and the phase unwrapping step of InSAR. Coalfield is the exact object providing such challenges for InSAR technique. Strong mining activities often induces large scale non-linear deformation with large gradient. This paper integrates offset tracking technique based on Corner Reflector (CR) and InSAR to overcome relevant problems. By applying offset tracking to high resolution TerraSAR-X intensity images, the coarse estimation of large deformation was obtained and extracted, allowing the following InSAR processing to carry out phase unwrapping correctly. Finally, the fine estimation of deformation was done by the Persistent Scatterer InSAR (PSI) technique. The detected deformation time series indicated good root-mean-square errors (RMSE), validated by GPS in situ investigation. All InSAR data were processed in the open source software StaMPS and one in-house InSAR package.

1 Introduction

Interferometric Synthetic Aperture Radar (InSAR) measures the phase differences between two or more SAR images over vast areas with high accuracy (Bamler and Hartl, 1998; Massonnet et al., 1993). In the past 10 years, various advanced InSAR techniques have been developed in order to detect slow deformation over a long time span or sudden displacements due to earthquakes and so on (Berardino et al., 2002; Lanari et al., 2004; Lu et al., 2004; Hooper et al., 2004; Kampes and Usai, 1999; Bechor, 2006; Li et al., 2011; Zhu and Bamler, 2010; Bachofer et al., 2014). The well-known methods Persistent Scatterers Interferometry (PSI) and Stanford Method for Persistent Scatterer (StaMPS), which perform analysis of "persistent scatterer" pixels on a succession of time-ordered images have been employed in different fields, both in urban and non-urban areas (Bachofer et al., 2014; Hooper et al., 2004; Liu et al., 2014; Raucoules et al., 2007a, b; Osmanoğlu et al., 2011). The interferogram time series techniques, e.g. Small BAseline Subset (SBAS), have also been proposed to estimate time-dependent deformation from InSAR data (Berardino et al., 2002; Lanari et al., 2004; Hooper, 2008). Based on a wavelet decomposition in space and a general parametrization in time, Multiscale InSAR Time Series (MInTS) focuses on unwrapped interferograms from a single viewing geometry, to measure the ground deformation (Hetland et al., 2012).

However exciting these developments are, InSAR techniques have some limitations and could not provide reliable results in some cases as expected. For instance, InSAR loses effectiveness in areas with large-gradient deformation due to the loss of coherence (Massonnet et al., 1993; Baran et al., 2005). In addition, considering correct phase unwrapping, the maximum phase gradient should not exceed 0.5 fringes per pixel (Spagnolini, 1995; Chen and Zebker, 2000). In coalfields, these limitations stop people from obtaining the full profile of mining-induced deformation. Mining subsidence hazard map might be derived but with the maximum subsidence parameter missing.

A number of methods have been proposed to solve large-gradient deformation problems in coalfield or other similar fields and have resulted in successful achievements, e.g. combining measurements from GPS and levelling, or using existing deformation records to help InSAR phase recovery (Simons et al., 2002; Bürgmann et al., 2006). Nevertheless, InSAR has to rely on other measurements in those cases, e.g. GPS, but not being a standalone technique for deformation monitoring.

Offset tracking method has been successfully applied to several studies for mapping glaciation, mining subsidence, landslides or co-seismic fault movements (Scambos et al., 1992; Strozzi et al., 2002; Giles et al., 2009; Zhao et al., 2013). Differing from PSI, offset tracking using the SAR amplitude is not able to evaluate some error components accurately, such as DEM errors, even though the SAR amplitude is little or even not affected by the atmospheric disturbances due to an independence on the use of phase values (Raucoules et al., 2013; Singleton et al., 2014). Suggested re-

SED
6, 2759–2778, 2014

construction of displacement and extraction before unwrapping phase was performed quite well in Tehran Basin (Sadeghi et al., 2013). Unfortunately, this works only when linear deformation component dominates in the InSAR phases. Some important work with regard to precise analysis of offset tracking integrated with SBAS analysis have been addressed successfully (Casu et al., 2011; Manconi and Casu, 2012). The so-called Pixel Offset (PO)-SBAS technique and relevant applications to volcanos have indicated a more correct evaluation than other techniques of mapping large deformation on the ground by satellite SAR (Manconi and Casu, 2012). Moreover, research about rapid measurements of landslides by PO approach was also well presented, which pointed out an exciting possibility for Earth hazards early warning system (Manconi et al., 2014).

In this paper, we proposed a StaMPS/InSAR approach integrated with offset tracking method by means of Corner Reflectors (CR). On one hand, considering that SAR sensors with short wavelength could decrease the maximum Detectable Deformation Gradient (DDG), it may be concluded that SAR images with long wavelength are more suitable for large-gradient deformation monitoring using phase measurements. In another respect, DDG might be increased by using high resolution SAR data through the much smaller pixel size. Moreover, TerraSAR-X has a much shorter revisit cycle (11 days or even shorter) than other SAR sensors, which dramatically increases the sampling rate of deformation monitoring. In this study, the approach was applied to a coal mining area by using the high resolution TerraSAR-X images and two time series of large-gradient and nonlinear deformation induced by mining excavation were extracted with centimetre-level precision validated by in situ investigation.

2 Methodology

Offset tracking deals with offsets of two SAR images and detects the pixel change in both range and azimuth directions when the normalized cross-correlation is performed on each pixel by using a moving window (Strozzi et al., 2002). For co-registration of images, oversampling factor of 2 was applied to the image patches to increase the estimation accuracy. By comparing the height of signal-to-noise ratio (SNR), the estimated offset with the highest SNR is selected to be the pixel offset value (Strozzi et al., 2002). The offsets are induced by two kinds of effects. The first kind is the global offsets, caused by slightly different radar look angle and orbital error. The second kind is local offsets, determined by displacements in two directions. In this algorithm, only the local offsets are used. Therefore, we determined the polynomial coefficients for offsets in both range and azimuth directions over the whole image, in order to estimate and remove the disturbance of offsets caused by the difference in radar imaging geometry. Moreover, the bilinear polynomial function determined over the whole image helps to remove the orbital offsets. In this study, only displacements in range direction was considered since mostly vertical deformation happens at the central area of a subsidence strata (He et al., 1991). In Fig. 1a, assume there is a data stack of SAR images.

$$\phi^{i}_{\mathrm{def},0}(k) = -\frac{4\pi}{\lambda}\mathrm{dis}^{i}_{\mathrm{rg},0}(k). \qquad (1)$$

$\phi^{i}_{\mathrm{def},0}(k)$ is the coarse estimation of deformation phase component of kth PS candidate on its slave image, while $\mathrm{dis}^{i}_{\mathrm{rg},0}(k)$ is the coarse estimate of range displacement of kth PS candidate on its slave image. Meanwhile, the DInSAR phase series $\boldsymbol{\psi} = [\psi_1, \psi_2, \cdots, \psi_{N-1}]$ and cross-correlation series $\boldsymbol{\gamma} = [\gamma_1, \gamma_2, \cdots, \gamma_{N-1}]$ of each PS candidate are generated. Furthermore, ahead of residual DEM estimation, the PS candidates are firstly selected based on Eq. (2).

$$\overline{\gamma} \geq S, \overline{\gamma} = \frac{1}{N-1}\sum_{i=1}^{N-1}\gamma_i. \qquad (2)$$

$\overline{\gamma}$ is the arithmetical average of the cross-correlation series generated from the previous step, and S is a predefined threshold.

The procedure of residual DEM estimation and PS reselection are then carried out in StaMPS (Hooper et al., 2004). StaMPS approach does not rely on any predefined

SED
6, 2759–2778, 2014

displacement model and thus is advantageous in terms of utilizing in monitoring natural phenomena. The topographic corrected phases of each reselected PS points are composed with several terms:

$$\psi^i_{\text{corrected}}(k) = W\left\{\phi^i_{\text{def}}(k) + \phi^i_{\text{atm}}(k) + \phi^i_{\text{orb}}(k) + \phi^i_{\text{noise}}(k)\right\}. \tag{3}$$

$W\{\cdot\}$ is the wrapping operator, $\psi_{\text{corrected}}$ means the wrapped topographic corrected phase. ϕ_{def} means the deformation phase term, ϕ_{atm} means the phase contributed to atmospheric effect, ϕ_{orb} denotes the phase component that results in inaccurate orbital data, while ϕ_{noise} represents the phase contribution generated from other noise terms. In the following step, the first estimation of deformation phase component is extracted from the topographic phase:

$$\begin{aligned}\psi^i_{\text{res}}(k) &= W\left\{\psi^i_{\text{corrected}}(k) - \phi^i_{\text{def},0}(k)\right\}\\ &= W\{\phi^i_{\text{def}}(k) - \phi^i_{\text{def},0}(k) + \phi^i_{\text{atm}}(k) + \phi^i_{\text{orb}}(k) + \phi^i_{\text{noise}}(k)\}.\end{aligned} \tag{4}$$

As long as the major part of deformation phase is extracted, the wrapped residual phase can be successfully unwrapped in spatial and temporal domains. Then, the coarse estimation of deformation phase is added back on the unwrapped residual phase to get the unwrapped topographic corrected phase $\phi^i_{\text{res}}(k)$:

$$\phi^i_{\text{corrected}} = \phi^i_{\text{res}}(k) + \phi^i_{\text{def},0}(k) = \phi^i_{\text{def}}(k) + \phi^i_{\text{atm}}(k) + \phi^i_{\text{orb}}(k) + \phi^i_{\text{noise}}(k). \tag{5}$$

In order to reconstruct the deformation series from the unwrapped topographic corrected phase, temporal and spatial domain filtering, using window 7 and 16 respectively were conducted. Since the atmosphere phase has the property of high-frequency in time and low-frequency in space, such filtering can estimate atmosphere phase. Subtracting this component from Eq. (5) leaves just ϕ^i_{def} and spatially uncorrelated error terms which can be modeled as noise. Using the separated ϕ^i_{def}, the deformation series can be generated.

Discussion Paper | Discussion Paper | Discussion Paper | Discussion Paper |

SED

6, 2759–2778, 2014

An improved approach to estimate large-gradient deformation

D. Liu et al.

3 Experiment area and SAR data

The Area Of Interest (AOI) of this study is located in Xishan coal mine, Gujiao city, Shanxi Province of China (Fig. 1b). It is the second largest coking coal mine of the world. Most of this area has large mountains with steep slopes and ravines which are mainly composed of Carboniferous, Permian sandstone, shale and Quaternary loess (Liu et al., 2013, 2014).

This area is full of trees, grasses and bushes which might bring a lot of coherence loss to InSAR observation. Heavy underground mining excavation is quite common in this coalfield inducing lots of surface deformation. According to previous study, the maximum subsidence can reach to meters in months.

Since the algorithm of offset estimation in this study is based on the intensity cross-correlation algorithm, the quality of SAR backscatter intensity images is the primary issue we have to take into account. Metallic trihedral corner reflectors with 1 m right-angle side were employed here because of its accurate measurement of backscatter coefficients along with GPS surveying (Fig. 1c and d) (Liu et al., 2014, 2013; Ye et al., 2004). Both the offset tracking and PSI are carried out on CR points and other PS candidates rather than on the whole image.

A total of 21 X-band TerraSAR-X images in strip map mode were acquired in 2012 for this study (Table 1). Most perpendicular baselines were between 3 m and 150 m, which mean they are obviously beneficial for deformation monitoring. A steep incidence angle of 26° was used to avoid strong shadow effects in this mountainous area.

4 Results and analysis

As discussed previously, the full definition of the DDG in terms of the coherence value is defined by the wavelength and the pixel size (Baran et al., 2005). It is naturally obvious to use small looks for mapping large-gradient deformation field. Therefore, the multilook number two was chosen in InSAR processing when single look lost most patterns. This InSAR result was then used for the comparison with the proposed novel method.

In this mountainous area full of vegetation, we are happy to see that CR could be detected on the amplitude map very clearly when the vicinity of the CR has low backscatter intensities (Fig. 2b and c). Therefore, both the co-registration and offset tracking procedure were assisted by using the precise location of CR.

Inteferometric processing profiles phase changes with time as presented in Fig. 3. Dense fringes in the flattened interferograms reflect the strong deformation on the ground induced by mining activities. In terms of the intensity of deformation, it even increased since more fringes observed in the interferogram of SAR pair 20120518–20120529, comparing to that in April 2012. More interferograms refer to (Liu et al., 2014). Offset tracking processing was done for all adjacent pairs among 21 TerraSAR-X images (Fig. 4). The dark and blue rectangles in Fig. 2a were selected to be two test sites as two CRs, numbered as CR1 and CR2 were available in each site. By selecting both CRs as PS candidates, the former processing was integrated into StaMPS processing chain. Employing high-pass filter in time then low-pass filter in space, and then modelling the spatially uncorrelated error terms, the time series of deformation at each site were estimated (Fig. 5a and b). In the whole InSAR processing, we assume that deformation happens only vertically at the subsidence strata. InSAR measurements are thus projected from line-of-sight to the vertically direction.

GPS observations were made for two CRs nearly every 11 days and were used to validate the both results derived from normal InSAR and integrated InSAR (Fig. 5). Apparently, the normal InSAR is not able to deal with the detection of maximum subsidence since the large-gradient deformation exceeds the maximum DDG and will result in phase unwrapping error. Normal offset tracking results indicate sudden subsidence signal which are attributed to strong mining excavation from April 2012 to June 2012. Since July 2012, CR2 has stabilized relatively as it did not locate in the subsidence basin centre any more. Comparing to the coarse estimated displacement series by normal offset tracking, the time series of integrated method are much smoother. When

SED
6, 2759–2778, 2014

validating the time series from integrated InSAR and GPS, impressive results with very few discrepancies – less than 5 cm at both points – are shown (Fig. 5). Such discrepancies may be induced by accurate of this approach itself, or the assumption that only vertical displacements were considered in this field. In total, this new approach detected cumulative subsidence of 2.048 m at CR1 and 2.639 m at CR2, from April to November 2012. Making the GPS observation as the truth value, the root-mean-square errors (RMSE) of time series derived by each method were reported in Table 2, which reflects the total difference of the methods with GPS measurements. The integrated InSAR approach indicates significant improvements of RMSE at both sites, comparing to InSAR and offset tracking methods.

This work has evaluated the possibility of mapping large deformation by integrating offset tracking approach and PSI in the open source package StaMPS, which is available to a larger research community. More exciting works are expected if apply this approach to other SAR sensors with high resolution, which is the key parameter for the accuracy of offset tracking approach (Jung et al., 2013). Nevertheless, CR is required in this hilly area with lots of vegetation to be a PS point for helping precise measurements, when most of other PS candidates are with low qualities. Moreover, 3-D measurements and rapid mapping ability in other proposed methodologies introduced above are also importance aspects of the future developments of our approach.

5 Conclusions

In this paper, the proposed offset tracking and PSI integrated approach demonstrated its capability of measuring large-gradient subsidence induced by coal mining activities where normal InSAR techniques always fail due to the DDG limitation and loss of coherence caused by heavy excavations. It was also inferred that we could benefit from high resolution SAR data and CR in the mountainous area. The important parameter of coal mining engineering, maximum subsidence (approximate 2 m in two months) was estimated in Xishan accurately by TerraSAR-X SAR data firstly. In terms of RMSE (< 0.1), the integrated approach indicated significant improvements. Along with the Subsidence Hazard Boundary (SHB) presented in the companion paper, full profiles of a mining subsidence could be provided (Liu et al., 2014).

As a main strength, this work was done based on the open source package StaMPS which is available to a larger research community, and one in-house software which is going to be open. 3-D measurements and rapid mapping ability in other proposed methodologies introduced above are importance aspects of the future developments of our approach. Moreover, the capability of working with new SAR missions with high resolution will be the way forward of this approach.

Acknowledgements. TerraSAR-X images were provided by DLR under the scientific proposal LAN1185. The field surveying was carried out and kindly provided by Mr. Zhenguo Liu in CUMT. Thanks for the developers of StaMPS. Their open mind made our work possible. Thanks for the fabulous plotting support from Mr. Jianlin Zhao in KU Leuven. Thanks go to Ms Armağan Güleç Korumaz for nice suggestions.

References

Bachofer, F., Quénéhervé, G., and Märker, M.: The Delineation of Paleo-Shorelines in the Lake Manyara Basin using TerraSAR-X data, Remote Sensing, 6, 2195–2212, 2014.

Bamler, R. and Hartl, P.: Synthetic aperture radar interferometry, Inverse probl., 14, R1, doi:10.1088/0266-5611/14/4/001, 1998.

Baran, I., Stewart, M., and Claessens, S.: A new functional model for determining minimum and maximum detectable deformation gradient resolved by satellite radar interferometry, IEEE T. Geosci. Remote, 43, 675–682, 2005.

Bechor, N.: Extending Interferometric Synthetic Aperture Radar Measurements from One to Two Dimensions, Stanford University, 2006.

Berardino, P., Fornaro, G., Lanari, R., and Sansosti, E.: A new algorithm for surface deformation monitoring based on small baseline differential SAR interferograms, IEEE T. Geosci. Remote, 40, 2375–2383, 2002.

Bürgmann, R., Hilley, G., Ferretti, A., and Novali, F.: Resolving vertical tectonics in the San Francisco Bay Area from permanent scatterer InSAR and GPS analysis, Geology, 34, 221–224, 2006.
Casu, F., Manconi, A., Pepe, A., and Lanari, R.: Deformation time-series generation in areas characterized by large displacement dynamics: the SAR amplitude pixel-offset SBAS technique, IEEE T. Geosci. Remote, 49, 2752–2763, 2011.
Chen, C. W. and Zebker, H. A.: Network approaches to two-dimensional phase unwrapping: intractability and two new algorithms, JOSA A, 17, 401–414, 2000.
Giles, A., Massom, R., and Warner, R.: A method for sub-pixel scale feature-tracking using Radarsat images applied to the Mertz Glacier Tongue, East Antarctica, Remote Sens. Environ., 113, 1691–1699, 2009.
He, G., Yang, L., and Ling, G.: Mining Subsidence, CUMT Press, Xuzhou, 1991.
Hetland, E., Musé, P., Simons, M., Lin, Y., Agram, P., and DiCaprio, C.: Multiscale InSAR time series (MInTS) analysis of surface deformation, J. Geophys. Res.-Sol. Ea., 117, B02404, doi:10.1029/2011JB008731, 2012.
Hooper, A.: A multi-temporal InSAR method incorporating both persistent scatterer and small baseline approaches, Geophys. Res. Lett., 35, L16302, doi:10.1029/2008GL034654, 2008.
Hooper, A., Zebker, H., Segall, P., and Kampes, B.: A new method for measuring deformation on volcanoes and other natural terrains using InSAR persistent scatterers, Geophys. Res. Lett., 31, L23611, doi:10.1029/2004GL021737, 2004.
Jung, H.-S., Lu, Z., and Zhang, L.: Feasibility of along-track displacement measurement from Sentinel-1 interferometric wide-swath mode, IEEE T. Geosci. Remote, 51, 573–578, 2013.
Kampes, B. and Usai, S.: Doris: The delft object-oriented radar interferometric software, 2nd International Symposium on Operationalization of Remote Sensing, Enschede, the Netherlands, p. 20, 1999.
Lanari, R., Lundgren, P., Manzo, M., and Casu, F.: Satellite radar interferometry time series analysis of surface deformation for Los Angeles, California, Geophys. Res. Lett., 31, L23613, doi:10.1029/2004GL021294, 2004.
Li, Z., Elliott, J. R., Feng, W., Jackson, J. A., Parsons, B. E., and Walters, R. J.: The 2010 MW 6.8 Yushu (Qinghai, China) earthquake: constraints provided by InSAR and body wave seismology, J. Geophys. Res.-Sol. Ea., 116, B10302, doi:10.1029/2011JB008358, 2011.

Liu, D., Shao, Y., Liu, Z., Riedel, B., Sowter, A., Niemeier, W., and Bian, Z.: Evaluation of InSAR and TomoSAR for Monitoring Deformations Caused by Mining in a Mountainous Area with High Resolution Satellite-Based SAR, Remote Sensing, 6, 1476–1495, 2014.

Liu, Z., Bian, Z., Lü, F., and Dong, B.: Monitoring on subsidence due to repeated excavation with DInSAR technology, Internat. J. Min. Sci. Technol., 23, 173–178, 2013.

Lu, Z., Rykhus, R., Masterlark, T., and Dean, K. G.: Mapping recent lava flows at Westdahl Volcano, Alaska, using radar and optical satellite imagery, Remote Sens. Environ., 91, 345–353, 2004.

Manconi, A. and Casu, F.: Joint analysis of displacement time series retrieved from SAR phase and amplitude: impact on the estimation of volcanic source parameters, Geophys. Res. Lett., 39, L14301, doi:10.1029/2012GL052202, 2012.

Manconi, A., Casu, F., Ardizzone, F., Bonano, M., Cardinali, M., De Luca, C., Gueguen, E., Marchesini, I., Parise, M., Vennari, C., Lanari, R., and Guzzetti, F.: Brief Communication: Rapid mapping of landslide events: the 3 December 2013 Montescaglioso landslide, Italy, Nat. Hazards Earth Syst. Sci., 14, 1835–1841, doi:10.5194/nhess-14-1835-2014, 2014.

Massonnet, D., Rossi, M., Carmona, C., Adragna, F., Peltzer, G., Feigl, K., and Rabaute, T.: The displacement field of the Landers earthquake mapped by radar interferometry, Nature, 364, 138–142, 1993.

Osmanoğlu, B., Dixon, T. H., Wdowinski, S., Cabral-Cano, E., and Jiang, Y.: Mexico City subsidence observed with persistent scatterer InSAR, Int. J. Appl. Earth Obs., 13, 1–12, 2011.

Raucoules, D., Bourgine, B., de Michele, M., Le Cozanet, G., Closset, L., Bremmer, C., Veldkamp, H., Tragheim, D., Bateson, L., and Crosetto, M.: Persistent scatterers interferometry independent validation and intercomparison of results – final report, BRGM/RP-55649-FR, 2007a.

Raucoules, D., Colesanti, C., and Carnec, C.: Use of SAR interferometry for detecting and assessing ground subsidence, CR Geosci., 339, 289–302, 2007b.

Raucoules, D., De Michele, M., Malet, J.-P., and Ulrich, P.: Time-variable 3D ground displacements from high-resolution synthetic aperture radar (SAR). Application to La Valette landslide (South French Alps), Remote Sens. Environ., 139, 198–204, 2013.

Sadeghi, Z., Valadan Zoej, M., and Dehghani, M.: An Improved Persistent Scatterer Interferometry for Subsidence Monitoring in the Tehran Basin, 2013.

SED
6, 2759–2778, 2014

Scambos, T. A., Dutkiewicz, M. J., Wilson, J. C., and Bindschadler, R. A.: Application of image cross-correlation to the measurement of glacier velocity using satellite image data, Remote Sens. Environ., 42, 177–186, 1992.
Simons, M., Fialko, Y., and Rivera, L.: Coseismic deformation from the 1999 M_w 7.1 Hector Mine, California, earthquake as inferred from InSAR and GPS observations, B. Seismol. Soc. Am., 92, 1390–1402, 2002.
Singleton, A., Li, Z., Hoey, T., and Muller, J.-P.: Evaluating sub-pixel offset techniques as an alternative to D-InSAR for monitoring episodic landslide movements in vegetated terrain, Remote Sens. Environ., 147, 133–144, 2014.
Spagnolini, U.: 2-D phase unwrapping and instantaneous frequency estimation, IEEE T. Geosci. Remote, 33, 579–589, 1995.
Strozzi, T., Luckman, A., Murray, T., Wegmuller, U., and Werner, C. L.: Glacier motion estimation using SAR offset-tracking procedures, IEEE T. Geosci. Remote, 40, 2384–2391, 2002.
Ye, X., Kaufmann, H., and Guo, X.: Landslide monitoring in the Three Gorges area using D-InSAR and corner reflectors, Photogramm. Eng. Rem. S., 70, 1167–1172, 2004.
Zhao, C., Lu, Z., and Zhang, Q.: Time-series deformation monitoring over mining regions with SAR intensity-based offset measurements, Remote Sensing Letters, 4, 436–445, 2013.
Zhu, X. X. and Bamler, R.: Very high resolution spaceborne SAR tomography in urban environment, IEEE T. Geosci. Remote, 48, 4296–4308, 2010.

SED
6, 2759–2778, 2014

Table 1. The parameters of the TerraSAR-X data in this study.

Sensor characteristics	Values
Frequency (GHz)	9.6
Wavelength (cm)	3.1
Polarisation	Horizontal–Horizontal
Swath width (km)	50
Incidence angle (degree)	~ 26
Range pixel spacing (m)	0.9
Azimuth pixel spacing (m)	1.9
Orbit repeat cycle (days)	11
Precise orbit accuracy (cm)	~ 10

SED
6, 2759–2778, 2014

Table 2. RMSE of different approaches comparing to GPS observation.

	Integrated InSAR	InSAR	Offset tracking
CR 1	0.069	1.62	0.169
CR 2	0.032	1.77	0.109

SED
6, 2759–2778, 2014

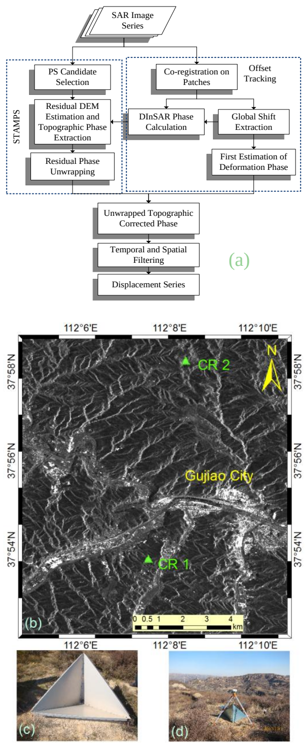

Figure 1. (a) Flow chart of the proposed approach presenting the integration of StaMPS and offset tracking; **(b)** the study area shown on a TerraSAR-X amplitude image, taken on 15 April 2012. Approximate location of two Corner Reflectors (CR) presented by green triangles; **(c, d)** photos of CR and relevant GPS survey at this coalfield.

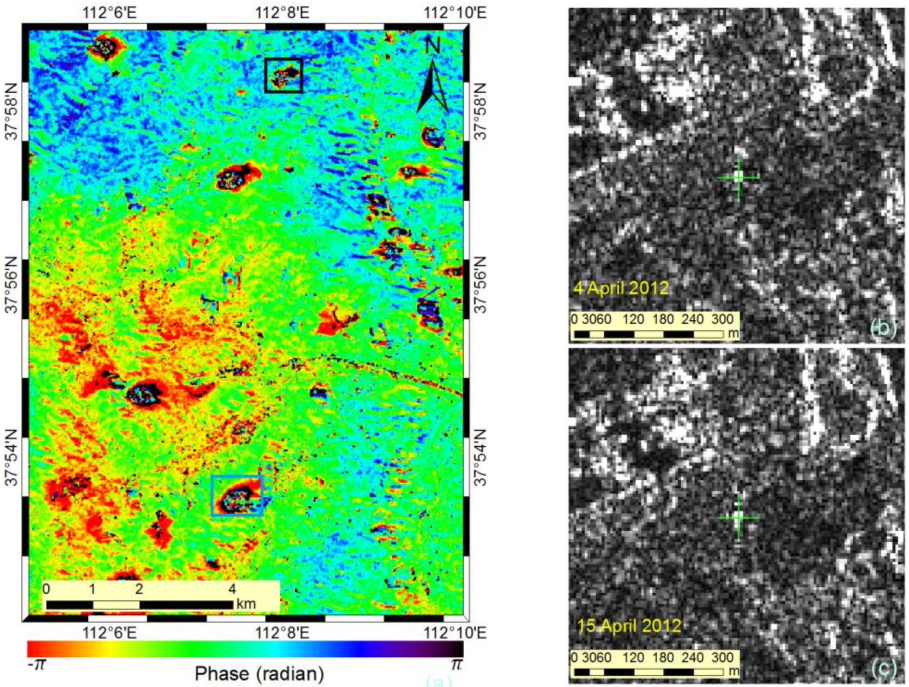

Figure 2. (a) Wrapped interferogram of AOI generated by TerraSAR-X images taken on 4 April 2012 and 15 April 2012, where the CR1 and CR2 locate in blue rectangle and dark rectangle, respectively; **(b, c)** a part of AOI taken from the blue rectangle area in **(a)**. The green cross locates CR1 on SAR intensity images taken on 4 April 2012 and 15 April 2012, respectively. The offset is then calculated to be 14 cm.

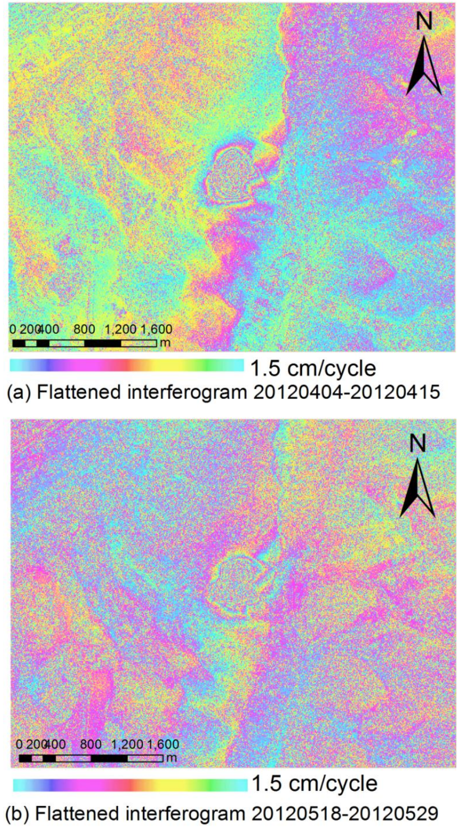

Figure 3. (a) flattened interferogram of SAR pair 20120404–20120415, **(b)** flattened interferogram of SAR pair 20120518–20120529. Image center coordinates: 37°53′35.51″ N, 112°07′35.25″ E. This area includes the region indicated by the blue rectangle in Fig. 2a.

SED
6, 2759–2778, 2014

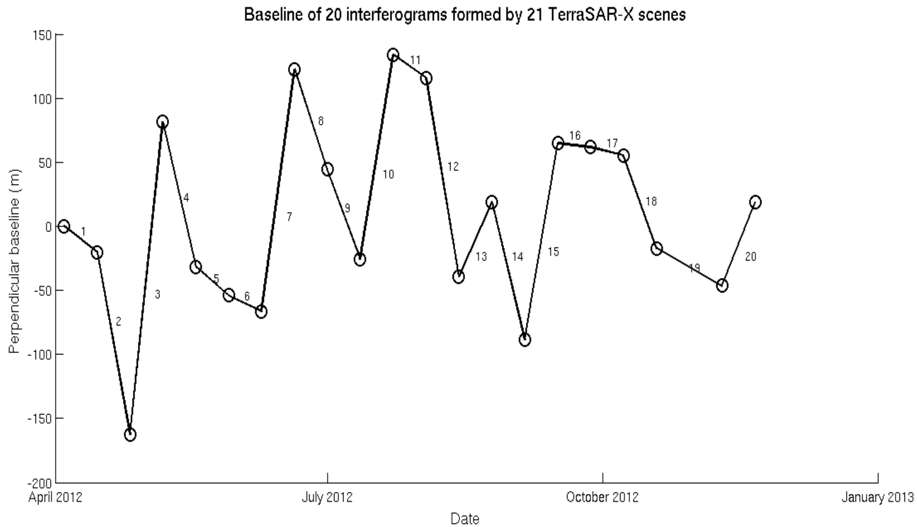

Figure 4. Interferogram pairs used in this study. Circles indicate SAR images while lines connecting them are baselines.

SED
6, 2759–2778, 2014

Title Page
Abstract Introduction
Conclusions References
Tables Figures
◀ ▶
Back Close
Full Screen / Esc
Printer-friendly Version
Interactive Discussion

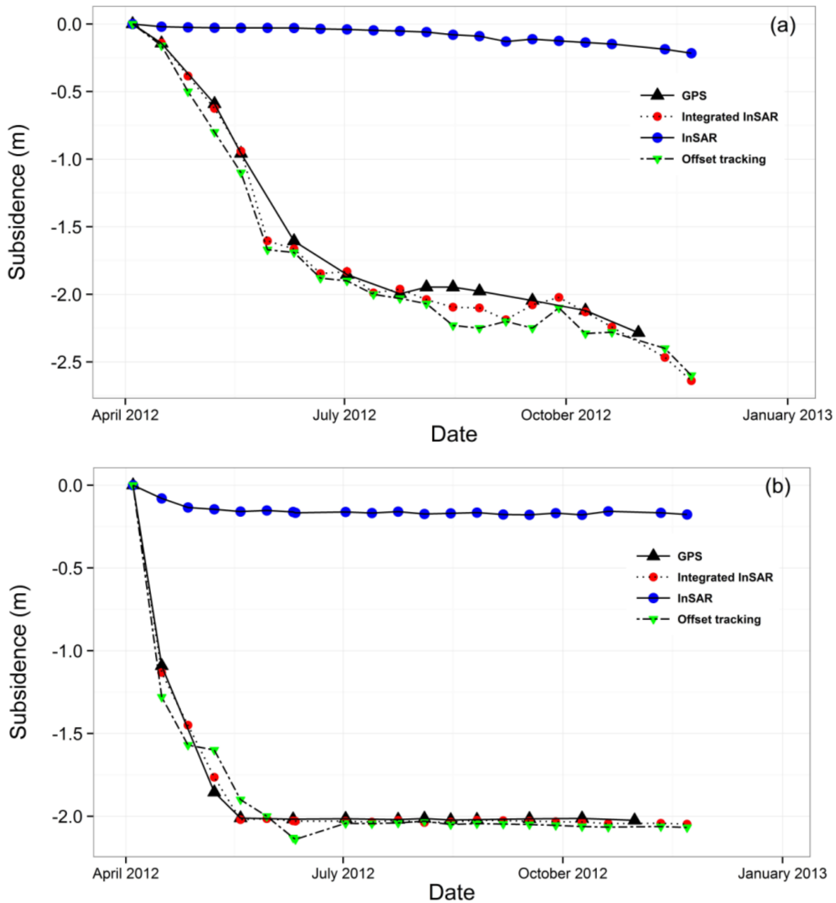

Figure 5. Time series of deformation derived from InSAR, offset tracking and integrated InSAR approach, with GPS validation. **(a)** time series at CR1; **(b)** time Series at CR2.